The Astrophysical Journal Letters, 894:L16 (5pp), 2020 May 10 https://doi.org/10.3847/2041-8213/ab8b59

Probing the Magnetic Field in the GW170817 Outflow Using H.E.S.S. Observations

H. Abdalla[1], R. Adam[2], F. Aharonian[3,4,5], F. Ait Benkhali[3], E. O. Angüner[6], M. Arakawa[7], C. Arcaro[1], C. Armand[8], T. Armstrong[9], H. Ashkar[10,41], M. Backes[1,11], V. Baghmanyan[12], V. Barbosa-Martins[13], A. Barnacka[14], M. Barnard[1], Y. Becherini[15], D. Berge[13], K. Bernlöhr[3], R. Blackwell[16], M. Böttcher[1], C. Boisson[17], J. Bolmont[18], S. Bonnefoy[13], J. Bregeon[19], M. Breuhaus[3], F. Brun[10], P. Brun[10], M. Bryan[20], M. Büchele[21], T. Bulik[22], T. Bylund[15], S. Caroff[18], A. Carosi[8], S. Casanova[3,12], M. Cerruti[18,42], T. Chand[1], S. Chandra[1], A. Chen[23], G. Cotter[9], M. Curyło[22], I. D. Davids[11], J. Davies[9], C. Deil[3], J. Devin[24], P. deWilt[16], L. Dirson[25], A. Djannati-Ataï[26], A. Dmytriiev[17], A. Donath[3], V. Doroshenko[27], J. Dyks[28], K. Egberts[29], F. Eichhorn[21], G. Emery[18], J.-P. Ernenwein[6], S. Eschbach[21], K. Feijen[16], S. Fegan[2], A. Fiasson[8], G. Fontaine[2], S. Funk[21], M. Füßling[13], S. Gabici[26], Y. A. Gallant[19], G. Giavitto[13], L. Giunti[26], D. Glawion[30], J. F. Glicenstein[10], D. Gottschall[27], M.-H. Grondin[24], J. Hahn[3], M. Haupt[13], G. Heinzelmann[25], G. Hermann[3], J. A. Hinton[3], W. Hofmann[3], C. Hoischen[29], T. L. Holch[31], M. Holler[32], M. Hörbe[9], D. Horns[25], D. Huber[32], H. Iwasaki[7], M. Jamrozy[14], D. Jankowsky[21], F. Jankowsky[30], A. Jardin-Blicq[3], V. Joshi[21], I. Jung-Richardt[21], M. A. Kastendieck[25], K. Katarzyński[33], M. Katsuragawa[34], U. Katz[21], D. Khangulyan[7], B. Khélifi[26], S. Klepser[13], W. Kluźniak[28], Nu. Komin[23], R. Konno[13], K. Kosack[10], D. Kostunin[13], M. Kreter[1], G. Lamanna[8], A. Lemière[26], M. Lemoine-Goumard[24], J.-P. Lenain[18], E. Leser[13,29], C. Levy[18], T. Lohse[31], I. Lypova[13], J. Mackey[4], J. Majumdar[13], D. Malyshev[27], D. Malyshev[21], V. Marandon[3], P. Marchegiani[23], A. Marcowith[19], A. Mares[24], G. Martí-Devesa[32], R. Marx[3], G. Maurin[8], P. J. Meintjes[35], R. Moderski[28], M. Mohamed[30], L. Mohrmann[21], C. Moore[36], P. Morris[9], E. Moulin[10], J. Muller[2], T. Murach[13], S. Nakashima[37], K. Nakashima[21], M. de Naurois[2], H. Ndiyavala[1], F. Niederwanger[32], J. Niemiec[12], L. Oakes[31], P. O'Brien[36], H. Odaka[38], S. Ohm[13,41], E. de Ona Wilhelmi[13], M. Ostrowski[14], M. Panter[3], R. D. Parsons[3], B. Peyaud[10], Q. Piel[8,41], S. Pita[26], V. Poireau[8], A. Priyana Noel[14], D. A. Prokhorov[20,23], H. Prokoph[13], G. Pühlhofer[27], M. Punch[15,26], A. Quirrenbach[30], S. Raab[21], R. Rauth[32], A. Reimer[32], O. Reimer[32], Q. Remy[19], M. Renaud[19], F. Rieger[3], L. Rinchiuso[10], C. Romoli[3], G. Rowell[16], B. Rudak[28], E. Ruiz-Velasco[3], V. Sahakian[39], S. Sailer[3], S. Saito[7], D. A. Sanchez[8], A. Santangelo[27], M. Sasaki[21], M. Scalici[27], R. Schlickeiser[40], F. Schüssler[10,41], A. Schulz[13], H. M. Schutte[1], U. Schwanke[31], S. Schwemmer[30], M. Seglar-Arroyo[10], M. Senniappan[15], A. S. Seyffert[1], N. Shafi[23], K. Shiningayamwe[11], R. Simoni[20], A. Sinha[26], H. Sol[17], A. Specovius[21], S. Spencer[9], M. Spir-Jacob[26], Ł. Stawarz[14], R. Steenkamp[11], C. Stegmann[29,13], C. Steppa[29], T. Takahashi[34], T. Tavernier[10], A. M. Taylor[13,41], R. Terrier[26], D. Tiziani[21], M. Tluczykont[25], L. Tomankova[21], C. Trichard[2], M. Tsirou[19], N. Tsuji[7], R. Tuffs[3], Y. Uchiyama[7], D. J. van der Walt[1], C. van Eldik[21], C. van Rensburg[1], B. van Soelen[35], G. Vasileiadis[19], J. Veh[21], C. Venter[1], P. Vincent[18], J. Vink[20], H. J. Völk[3], T. Vuillaume[8], Z. Wadiasingh[1], S. J. Wagner[30], J. Watson[9], F. Werner[3], R. White[3], A. Wierzcholska[12,30], R. Yang[3], H. Yoneda[34], M. Zacharias[1], R. Zanin[3], A. A. Zdziarski[28], A. Zech[17], J. Zorn[3], N. Żywucka[1]

(H.E.S.S. Collaboration), and

X. Rodrigues[13,41]

[1] Centre for Space Research, North-West University, Potchefstroom 2520, South Africa
[2] Laboratoire Leprince-Ringuet, École Polytechnique, CNRS, Institut Polytechnique de Paris, F-91128 Palaiseau, France
[3] Max-Planck-Institut für Kernphysik, P.O. Box 103980, D-69029 Heidelberg, Germany
[4] Dublin Institute for Advanced Studies, 31 Fitzwilliam Place, Dublin 2, Ireland
[5] High Energy Astrophysics Laboratory, RAU, 123 Hovsep Emin St., Yerevan 0051, Armenia
[6] Aix Marseille Université, CNRS/IN2P3, CPPM, Marseille, France
[7] Department of Physics, Rikkyo University, 3-34-1 Nishi-Ikebukuro, Toshima-ku, Tokyo 171-8501, Japan
[8] Laboratoire d'Annecy de Physique des Particules, Univ. Grenoble Alpes, Univ. Savoie Mont Blanc, CNRS, LAPP, F-74000 Annecy, France
[9] University of Oxford, Department of Physics, Denys Wilkinson Building, Keble Road, Oxford OX1 3RH, UK
[10] IRFU, CEA, Université Paris-Saclay, F-91191 Gif-sur-Yvette, France
[11] University of Namibia, Department of Physics, Private Bag 13301, Windhoek 12010, Namibia
[12] Instytut Fizyki Jądrowej PAN, ul. Radzikowskiego 152, 31-342 Kraków, Poland
[13] DESY, D-15738 Zeuthen, Germany
[14] Obserwatorium Astronomiczne, Uniwersytet Jagielloński, ul. Orla 171, 30-244 Kraków, Poland
[15] Department of Physics and Electrical Engineering, Linnaeus University, SE-351 95 Växjö, Sweden
[16] School of Physical Sciences, University of Adelaide, Adelaide, SA 5005, Australia
[17] LUTH, Observatoire de Paris, PSL Research University, CNRS, Université Paris Diderot, 5 Place Jules Janssen, F-92190 Meudon, France
[18] Sorbonne Université, Université Paris Diderot, Sorbonne Paris Cité, CNRS/IN2P3, Laboratoire de Physique Nucléaire et de Hautes Energies, LPNHE, 4 Place Jussieu, F-75252 Paris, France
[19] Laboratoire Univers et Particules de Montpellier, Université Montpellier, CNRS/IN2P3, CC 72, Place Eugène Bataillon, F-34095 Montpellier Cedex 5, France
[20] GRAPPA, Anton Pannekoek Institute for Astronomy, University of Amsterdam, Science Park 904, NL-1098 XH Amsterdam, The Netherlands
[21] Friedrich-Alexander-Universität Erlangen-Nürnberg, Erlangen Centre for Astroparticle Physics, Erwin-Rommel-Str. 1, D-91058 Erlangen, Germany
[22] Astronomical Observatory, The University of Warsaw, Al. Ujazdowskie 4, 00-478 Warsaw, Poland
[23] School of Physics, University of the Witwatersrand, 1 Jan Smuts Avenue, Braamfontein, Johannesburg 2050 South Africa
[24] Université Bordeaux, CNRS/IN2P3, Centre d'Études Nucléaires de Bordeaux Gradignan, F-33175 Gradignan, France
[25] Universität Hamburg, Institut für Experimentalphysik, Luruper Chaussee 149, D-22761 Hamburg, Germany
[26] APC, AstroParticule et Cosmologie, Université Paris Diderot, CNRS/IN2P3, CEA/Irfu, Observatoire de Paris, Sorbonne Paris Cité, 10, rue Alice Domon et Léonie Duquet, F-75205 Paris Cedex 13, France
[27] Institut für Astronomie und Astrophysik, Universität Tübingen, Sand 1, D-72076 Tübingen, Germany
[28] Nicolaus Copernicus Astronomical Center, Polish Academy of Sciences, ul. Bartycka 18, 00-716 Warsaw, Poland
[29] Institut für Physik und Astronomie, Universität Potsdam, Karl-Liebknecht-Strasse 24/25, D-14476 Potsdam, Germany
[30] Landessternwarte, Universität Heidelberg, Königstuhl, D-69117 Heidelberg, Germany
[31] Institut für Physik, Humboldt-Universität zu Berlin, Newtonstr. 15, D-12489 Berlin, Germany

[32] Institut für Astro- und Teilchenphysik, Leopold-Franzens-Universität Innsbruck, A-6020 Innsbruck, Austria
[33] Centre for Astronomy, Faculty of Physics, Astronomy and Informatics, Nicolaus Copernicus University, Grudziadzka 5, 87-100 Torun, Poland
[34] Kavli Institute for the Physics and Mathematics of the Universe (WPI), The University of Tokyo Institutes for Advanced Study (UTIAS), The University of Tokyo, 5-1-5 Kashiwa-no-Ha, Kashiwa, Chiba 277-8583, Japan
[35] Department of Physics, University of the Free State, P.O. Box 339, Bloemfontein 9300, South Africa
[36] Department of Physics and Astronomy, The University of Leicester, University Road, Leicester LE1 7RH, UK
[37] RIKEN, 2-1 Hirosawa, Wako, Saitama 351-0198, Japan
[38] Department of Physics, The University of Tokyo, 7-3-1 Hongo, Bunkyo-ku, Tokyo 113-0033, Japan
[39] Yerevan Physics Institute, 2 Alikhanian Brothers St., 375036 Yerevan, Armenia
[40] Institut für Theoretische Physik, Lehrstuhl IV: Weltraum und Astrophysik, Ruhr-Universität Bochum, D-44780 Bochum, Germany
Received 2020 March 7; revised 2020 April 20; accepted 2020 April 20; published 2020 May 7

Abstract

The detection of the first electromagnetic counterpart to the binary neutron star (BNS) merger remnant GW170817 established the connection between short γ-ray bursts and BNS mergers. It also confirmed the forging of heavy elements in the ejecta (a so-called kilonova) via the r-process nucleosynthesis. The appearance of nonthermal radio and X-ray emission, as well as the brightening, which lasted more than 100 days, were somewhat unexpected. Current theoretical models attempt to explain this temporal behavior as either originating from a relativistic off-axis jet or a kilonova-like outflow. In either scenario, there is some ambiguity regarding how much energy is transported in the nonthermal electrons versus the magnetic field of the emission region. Combining the Very Large Array (radio) and Chandra (X-ray) measurements with observations in the GeV–TeV domain can help break this ambiguity, almost independently of the assumed origin of the emission. Here we report for the first time on deep H.E.S.S. observations of GW170817/GRB 170817A between 124 and 272 days after the BNS merger with the full H.E.S.S. array of telescopes, as well as on an updated analysis of the prompt (<5 days) observations with the upgraded H.E.S.S. phase-I telescopes. We discuss implications of the H.E.S.S. measurement for the magnetic field in the context of different source scenarios.

Unified Astronomy Thesaurus concepts: Gamma-ray transient sources (1853); Stellar mergers (2157); Gamma-ray bursts (629); Gamma-ray astronomy (628); Ejecta (453)

1. Introduction

The gravitational-wave (GW) event detected on 2017 August 17 by the advanced LIGO and Virgo detectors resulted from the merger of two neutron stars (NSs). The GW signal was followed after ~2 s by a short, low-luminosity γ-ray burst (GRB) and seen by the Fermi-GBM (Goldstein et al. 2017) and International Gamma-Ray Astrophysics Laboratory-Space Platform Interferometry (Savchenko et al. 2017) instruments. Observations in the optical band later associated this GRB (GRB 170817A) as the counterpart of GW170817 and localized it to the host galaxy NGC 4993 (Coulter et al. 2017). The fading UV, optical, and infrared radiation was followed by a rising nonthermal radio and X-ray signal after ~9 days (Troja et al. 2017). This behavior, as predicted by Takami et al. (2014), is indicative of efficient particle acceleration in the NS merger remnant and subsequent synchrotron emission of accelerated electrons in the ejecta's magnetic field.

After ~160 days, the synchrotron radiation started to plateau and later fade (Figure 1). This is similar to the behavior of a young supernova remnant, and suggests that the ejecta is transitioning from the free expansion to the Sedov–Taylor phase when the ejected mass of the merger remnant equals the swept-up circumstellar material.

Rodrigues et al. (2019) infer a total kinetic energy in the ejecta of 10^{51} erg, implying a total number of electrons in the remnant of 10^{55}. Accelerated electrons should also scatter off the intense radio and X-ray synchrotron radiation field and produce synchrotron self-Compton (SSC) emission. The expected peak energy of the SSC component depends on the maximum accelerated electron energy as probed by the X-rays. While the radio to X-ray emission probes the product of energy in electrons, u_e, and energy in magnetic fields, u_B, the SSC component is proportional to $u_e^2 \cdot u_B$. As shown by Takami et al. (2014) and Rodrigues et al. (2019), observations in the γ-ray regime can break the ambiguity between u_B and u_e and provide crucial insight into the magnetic field in the ejecta as well as the maximum accelerated particle energy.

In this work, we present deep H.E.S.S. observations of GW170817/GRB 170817A covering the peak and onset of fading in the X-ray and radio lightcurves from 124 to 272 days after the merger. This measurement is accompanied by an improved analysis of the H.E.S.S. data taken on the early (up to 5 day) kilonova. In the next section we present the H.E.S.S. data set and results, followed by a discussion on the implied magnetic field strength in a non-relativistic kilonova scenario and a relativistic jet scenario. Throughout this work we adopt a distance to the host galaxy NGC 4993 of 41.0 Mpc, corresponding to a redshift of $z = 0.009727$ (Hjorth et al. 2017).[43]

2. Data Analysis and Results

The data set was obtained from observations with the H.E.S.S. phase II array, including the upgraded 12 m diameter CT1-4 telescopes (Ashton et al. 2020) and the large 28 m diameter CT5 telescope. The analysis presented by Abdalla et al. (2017) used monoscopic data of the 28 m telescope

[41] Authors to whom any correspondence should be addressed at contact.hess@hess-experiment.eu.
[42] Now at Institut de Ciències del Cosmos (ICC UB), Universitat de Barcelona (IEEC-UB), Martí Franquès 1, E-08028 Barcelona, Spain.
[43] At this distance, very-high-energy (VHE; 100 GeV < E < 100 TeV) photons pair-produce $e^{\pm}$ in interactions with the extragalactic background light (EBL) on their way from GW170817 to Earth. The VHE flux reduction due to the EBL is energy dependent and varies between 10% and 30% between 1 and 10 TeV, respectively, assuming the Franceschini et al. (2008) EBL model. Note that the model curves have been derived ignoring the EBL correction.

Table 1
Properties of the H.E.S.S. Data Sets on GW170817/GRB 170817A and Analysis Results

Data Set	Configuration	$T - T_0$ (days)	Exposure (hr)	Energy Range (TeV)	$F(>E_{\rm th})$ (erg cm^{-2} s^{-1})	F(1–10 TeV) (erg cm^{-2} s^{-1})	Zenith Angle (deg)	Reference
I	CT 5	0.22–5.23	3.2	0.27–8.55	$<1.5 \times 10^{-12}$	...	58	Abdalla et al. (2017)
II	CT 1–5	0.22–5.23	3.2	0.56–17.8	$<4.7 \times 10^{-12}$	$<2.8 \times 10^{-12}$	58	This work
III	CT 1–5	124–272	53.9	0.13–23.7	$<1.6 \times 10^{-12}$	$<3.2 \times 10^{-13}$	24	This work

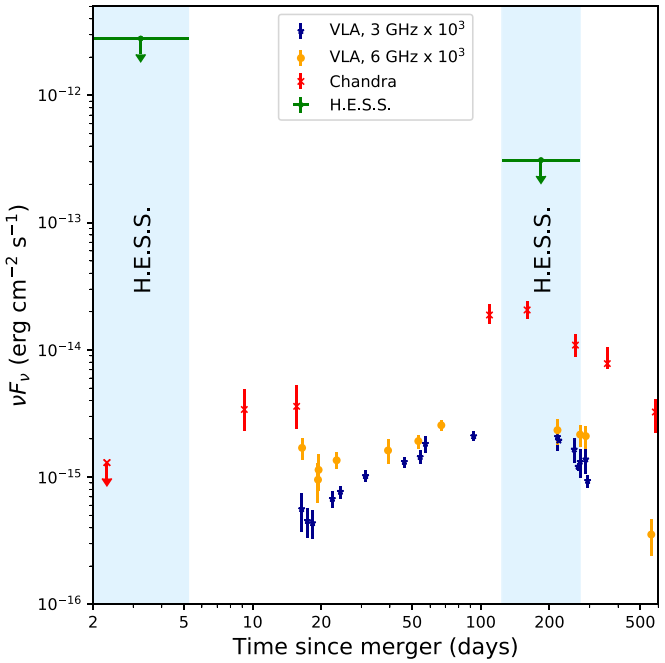

Figure 1. Shown are the H.E.S.S. observation windows (blue areas), VLA radio data at 3 GHz (blue stars) and 6 GHz (orange circles; Alexander et al. 2017, 2018; Hallinan et al. 2017; Dobie et al. 2018; Margutti et al. 2018; Mooley et al. 2018; Hajela et al. 2019), as well as X-ray data (red crosses; Nynka et al. 2018; Hallinan et al. 2017, and references therein). The H.E.S.S. 1–10 TeV energy flux upper limits (green arrows) are derived for the prompt and the long-term follow-up with CT1-5 (see Table 1).

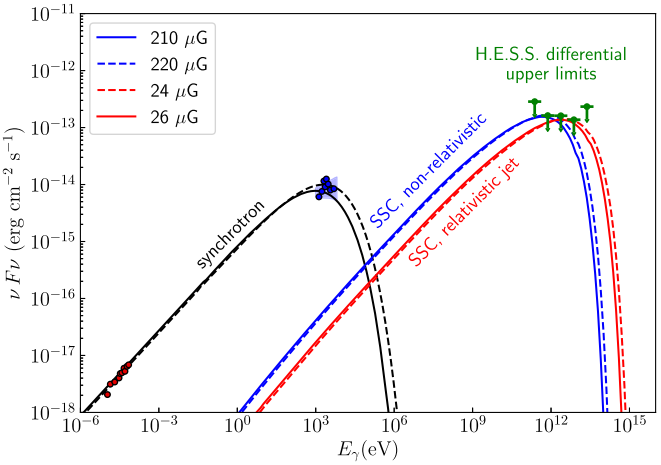

Figure 2. Spectra predicted by the SSC modeling of the remnant of GRB 170817A, 110 days after the merger, for two distinct assumptions on the geometry and expansion speed of the remnant: an isotropic, non-relativistic expansion (blue SSC curves) and a relativistic jet (red SSC curves). For both assumptions, we show the minimum magnetic field strength imposed by the H.E.S.S. upper limits (green arrows). Solid and dashed curves are obtained by considering respectively the minimum and maximum flux values allowed by the X-ray measurements (blue points), while retaining compatibility with the radio data (red points).

obtained between 5.3 hr and 5.3 days after the binary neutron star (BNS) merger. Here we extend this analysis to also include data taken with CT1-4. Observations from 2017 December to 2018 May with telescopes pointing 0.°5 offset from GW170817 were conducted allowing for simultaneous estimation of the background level in the signal region as discussed below. The different data sets are summarized in Table 1. A standard data quality selection is applied to the data (Aharonian et al. 2006; H.E.S.S. Collaboration et al. 2017). The events have been selected and their direction and energy reconstructed using a Monte Carlo, template-based, shower model technique (Parsons & Hinton 2014), requiring at least two telescope to see the same γ-ray event. With this method, an energy resolution of $\sim$10% and angular resolution (at 68% containment radius) of 0.°08 above γ-ray energies of 200 GeV is achieved. The resulting energy threshold of data set III is $E_{\rm th} = 130$ GeV. We define a circular region-of-interest centered on the optical position of GW170817 (Coulter et al. 2017) with a radius of 0.°09 for data sets II and III—hereafter referred to as the ON region. Ten to twenty background control regions (OFF regions) are defined radially symmetric with respect to the telescope pointing position for each observation (Fomin et al. 1994). This technique assures that the γ-ray signal and background are estimated with the same acceptance and under the same observation conditions. No significant γ-ray excess above the expected background is detected from the direction of GW170817 in any data set. A second analysis using an independent event calibration and reconstruction (de Naurois & Rolland 2009) confirms the result. A search for significant emission on monthly timescales also does not reveal any signal. For the total data set, 95% confidence level (C.L.) upper limits on the photon flux are derived using the method described by Rolke et al. (2005) and assuming an underlying power-law spectral index of the γ-ray emission of $\alpha = -2.0$ (see Rodrigues et al. 2019). Note that systematic errors are subdominant compared to statistical uncertainties when deriving upper limits, and are hence not considered here. All results are summarized in Table 1.

Figure 1 depicts the radio and X-ray flux measurements along with the inferred H.E.S.S. energy flux upper limits in the 1–10 TeV energy range for data sets II and III. Figure 2 shows the inferred energy flux upper limits at the 95% C.L. in the VHE γ-ray range from GRB 170817A for data set III, which has the best sensitivity at TeV energies. In the next section we discuss how the H.E.S.S. results constrain the magnetic field in the GW170817 ejecta in a jet and in a kilonova scenario.

3. Discussion

Recent detections of VHE emission from GRBs over minutes (Mirzoyan 2019) and hours (de Naurois 2019) motivate the search for very late time emission from GRB-related events, like

the remnant of GW170817. The H.E.S.S. differential upper limits can be translated into an integral energy flux limit, for a given assumption on the spectrum of the radiating particles. In turn, this limit provides a constraint on the magnetic field strength under the assumption of one-zone synchrotron emission with corresponding inverse Compton (IC) emission.

Observational evidence suggests that at early times, the kilonova provides the dominant target radiation field in the remnant (Villar et al. 2017). However, the decay of this component, whose flux falls steeply with $t^{-2.3}$, results in a late-time dominance of the synchrotron radiation in the source. It is therefore naturally expected that at late times SSC will dominate the remnant's IC emission.

The measured X-ray flux of the source can be used to infer the X-ray luminosity emitted as synchrotron radiation, L_X. In order to consistently model the emission from this electron population, a geometry assumption is necessary. We consider two scenarios: one where the remnant expands isotropically and non-relativistically, and the other where a relativistic jet is launched.

In the isotropic scenario, we assume a volume-filled spherical emitter with radius $R_{\rm iso} = \beta c \Delta t$, where $\Delta t = 110$ days is the time since the merger.[44] Based on photospheric velocity measurements of the remnant (Piro & Kollmeier 2018), we consider a value of the expansion speed of $\beta = 0.2$.

In the relativistic scenario, we consider a jet with speed $\beta = 0.94$ (corresponding to a Lorentz factor of $\Gamma = 3$) at late times, and a jet opening angle[45] of $\theta'_{\rm jet} = 5°$, observed at an angle of $\theta_{\rm obs} = 20° \approx 180°/\pi\Gamma$ from the jet axis; the source is therefore observed with a Doppler factor $\delta = \Gamma = 3$. These parameter values are motivated by radio observations of superluminal motion of the source (Mooley et al. 2018). Furthermore, from a purely theoretical standpoint, this value of the Lorentz factor is expected at $\sim$100 day timescales, considering the energy transfer from the shock into a surrounding medium of constant density (Rees & Meszaros 1992). The emitting region is assumed to be a spherical blob at the front edge of the jet, whose radius is therefore given by $R'_{\rm blob} \approx \delta\beta c \Delta t \theta'_{\rm jet}$.

The maximum energy of the emitted synchrotron radiation is fixed by X-ray observations, $E_{\rm X} \approx 10$ keV (Nynka et al. 2018). This is related to the magnetic field strength in the source, B', and the maximum electron energy of the emitting electrons, $E'_e = \delta^{-1} E_e$, through $E'_{\rm X} \propto E'^2_e B'$. This means that in the relativistic scenario, for a given value of B', the maximum energy of the emitting electrons scales as $E'_e \propto \delta^{-0.5}$. Furthermore, since the jet blob emits isotropically in its own rest frame, the X-ray luminosity, obtained assuming the observed emission is isotropic, $L_X^{\rm iso}$ deduced from flux measurements relates to the luminosity in the rest frame of the blob L'_X through $L_{\rm X}^{\rm iso} = \delta^4 L'_X$. This luminosity relates to the total number of X-ray-emitting electrons, N'_e, as well as E'_e and B', through $L'_{\rm X} = N'_e E'_e / \tau'_{\rm syn}(E'_e) \propto N'_e E'^2_e B'^2$, where $\tau'_{\rm syn}(E'_e)$ is the synchrotron cooling timescale. Therefore, in the relativistic jet scenario, for a given value of B' and measured X-ray flux, the number of electrons scales as $N'_e \propto \delta^{-3}$. This will affect the results of the SSC model, since for higher values of δ there will be fewer emitting electrons, and a lower density of synchrotron photons, thus reducing the expected γ-ray flux.

The γ-ray luminosity expected from SSC is given in the shock rest frame by $L'_{\rm IC} = N'_e E'_e / \tau'_{\rm IC}(E'_e) \propto N'_e (L'_{\rm X}/(4\pi R'^2 c)) E'^{0.5}_e$, where $\tau'_{\rm IC}(E'_e)$ is the IC cooling timescale, and R' is the size of the emitting region (either $R'_{\rm blob}$ or $R'_{\rm iso}$, defined above). The approximate scaling with $E'^{0.5}_e$ is due to the fact that the IC cooling occurs deep in the Klein–Nishina regime (since the observed synchrotron spectrum peaks at X-ray energies and the Lorentz factor of the ejecta is mild). Putting together the scalings given previously, we obtain that for a given value of B', the IC emission for the relativistic jet scenario scales as $L'_{IC} \propto \theta'^{-2}_{\rm jet} (\beta \Delta t)^{-2} \delta^{-9.25}$ in the shock rest frame, which corresponds to a luminosity in the observer's frame of

$$L_{\rm IC} \approx 10^{46} \left(\frac{\theta'_{\rm jet}}{5°}\right)^{-2} \left(\frac{\beta \Delta t}{0.94 \times 110 \text{ days}}\right)^{-2} \left(\frac{\delta}{3}\right)^{-5.25} \text{erg s}^{-1}. \quad (1)$$

Thus, a slower expansion of the emission region would lead to a more compact source and therefore a stronger constraint on the magnetic field strength (both in the jet-like and isotropic scenarios).

In Figure 2 we show the modeled synchrotron emission spectrum (black curves) and the respective SSC emission for both scenarios introduced above. These spectra were obtained with a numerical radiation model, introduced by Rodrigues et al. (2019). In this model, a population of electrons is considered to fill homogeneously the emission region, and to be continuously accelerated to a power-law spectrum, with a possible cutoff at the highest energies. As can be seen in Figure 2, these characteristics can explain radio (red points) and X-ray observations (blue points and blue shaded region). The parameters of the electron population have then been adjusted, and the magnetic field strength minimized, so that the predicted SSC emission does not exceed any of the 95% C.L. upper limits in the VHE γ-ray range derived from the H.E.S.S. observations (green). The solid versus dashed curves represent the two extreme cases consistent with the observed X-ray and radio fluxes. In the non-relativistic scenario, the H.E.S.S. limits can constrain the minimum magnetic field strength to $\gtrsim$210 μG. In contrast, in more highly relativistic scenarios, the lower limit is weakened to the level of $\gtrsim$24 μG. The reason is that the strong scaling of the SSC flux with the Doppler factor (Equation (1)) implies that for a more relativistic outflow, a higher electron number is necessary to reach the flux limits, which implies a lower magnetic field in order to maintain the X-ray flux.

As a point of comparison with the lower limit obtained through this analysis, the minimum magnetic field expected at late times downstream of the shock is of the order of $\sim 100 (\Gamma/3)(B_{\rm ISM}/10\ \mu\text{G})\ \mu$G (Kumar et al. 2012), where $B_{\rm ISM}$ is the magnetic field strength in the interstellar medium (ISM). Furthermore, observations of the prompt emission of GRB 080916C by Fermi-LAT and 1 day afterglow emission in X-rays and optical wavelengths have provided evidence of magnetic fields in the shock that are at the level of the compressed surrounding medium (Kumar & Duran 2009), thus suggesting an ISM magnetic field of $\sim$10 μG.

Very-high-energy γ-ray observations can provide a direct probe of the magnetic field in BNS merger remnants. While the

[44] We base this discussion on the 110 day timescale, for which there are quasi-simultaneous flux measurements in both radio and X-ray bands. As shown in Figure 1, the flux levels at this timescale are comparable throughout the H.E.S.S. observation window.

[45] Throughout this text, primed quantities denote parameter values in the shock rest frame and unprimed ones in the observer's frame.

radio and X-ray data constrain the synchrotron part of the nonthermal spectrum, a measurement of the IC component in γ-rays is needed to break the ambiguity between energy in electrons and magnetic fields. Interferometric radio observations and long-term X-ray observations are crucial for inferring the jet properties such as the opening angle, viewing angle, or the Doppler factor. Based on the GW170817/GRB 170817A characteristics, one other short GRB may have been seen off-axis (GRB 150101B; Troja et al. 2018). Long-term monitoring of BNS mergers in the radio, X-ray, and γ-ray domain is necessary to further constrain the source properties and bridge the gap between the early-time kilonova and nonthermal GRB emission on the one hand, and the long-term behavior and the interaction between the jet and the ISM on the other hand. Current-generation Imaging Atmospheric Cerenkov Telescopes such as H.E.S.S., MAGIC, or VERITAS can search for and study γ-ray counterparts on days-to-month timescales for BNS merger remnants seen under different viewing angles. Furthermore, the future Cerenkov Telescope Array (CTA) will be an order of magnitude more sensitive at around 1 TeV, allowing us to constrain the minimum magnetic field in events like GW170817/GRB 170817A to the mG regime. This will allow CTA to detect VHE γ-ray emission from events such as GW170817. As noted previously by Rodrigues et al. (2019), future observations may also be able to better constrain the nature of the nonthermal electrons. One possibility is that the observed radiation is dominated by "fresh" electrons picked up from the surroundings of the merger and accelerated at the shock front, allowing for hard photon spectra into the gamma-ray range. In a different scenario, the emission might originate in "old" electrons, continuously accelerated inside the volume of the ejecta, leading to cooling features at high energies.

The support of the Namibian authorities and of the University of Namibia in facilitating the construction and operation of H.E.S.S. is gratefully acknowledged, as is the support by the German Ministry for Education and Research (BMBF), the Max Planck Society, the German Research Foundation (DFG), the Helmholtz Association, the Alexander von Humboldt Foundation, the French Ministry of Higher Education, Research and Innovation, the Centre National de la Recherche Scientifique (CNRS/IN2P3 and CNRS/INSU), the Commissariat à l'Énergie atomique et aux Énergies alternatives (CEA), the U.K. Science and Technology Facilities Council (STFC), the Knut and Alice Wallenberg Foundation, the National Science Centre, Poland grant No. 2016/22/M/ST9/00382, the South African Department of Science and Technology and National Research Foundation, the University of Namibia, the National Commission on Research, Science & Technology of Namibia (NCRST), the Austrian Federal Ministry of Education, Science and Research and the Austrian Science Fund (FWF), the Australian Research Council (ARC), the Japan Society for the Promotion of Science and by the University of Amsterdam. We appreciate the excellent work of the technical support staff in Berlin, Zeuthen, Heidelberg, Palaiseau, Paris, Saclay, Tübingen, and in Namibia in the construction and operation of the equipment. This work benefited from services provided by the H.E.S.S. Virtual Organization, supported by the national resource providers of the EGI Federation. X.R. was supported by the Initiative and Networking Fund of the Helmholtz Association.

References

Abdalla, H., Abramowski, A., Aharonian, F., et al. 2017, ApJL, 850, L22
Aharonian, F., Akhperjanian, A. G., Bazer-Bachi, A. R., et al. 2006, A&A, 457, 899
Alexander, K. D., Berger, E., Fong, W., et al. 2017, ApJL, 848, L21
Alexander, K. D., Margutti, R., Blanchard, P. K., et al. 2018, ApJL, 863, L18
Ashton, T., Backes, M., Balzer, A., et al. 2020, APh, 118, 102425
Coulter, D. A., Foley, R. J., Kilpatrick, C. D., et al. 2017, Sci, 358, 1556
de Naurois, M. 2019, ATel, 13052, 1
de Naurois, M., & Rolland, L. 2009, APh, 32, 231
Dobie, D., Kaplan, D. L., Murphy, T., et al. 2018, ApJL, 858, L15
Fomin, V. P., Stepanian, A. A., Lamb, R. C., et al. 1994, APh, 2, 137
Franceschini, A., Rodighiero, G., & Vaccari, M. 2008, A&A, 487, 837
Goldstein, A., Veres, P., Burns, E., et al. 2017, ApJL, 848, L14
Hajela, A., Margutti, R., Alexander, K. D., et al. 2019, ApJL, 886, L17
Hallinan, G., Corsi, A., Mooley, K. P., et al. 2017, Sci, 358, 1579
H.E.S.S. Collaboration, Abdalla, H., Abramowski, A., et al. 2017, A&A, 600, A89
Hjorth, J., Levan, A. J., Tanvir, N. R., et al. 2017, ApJL, 848, L31
Kumar, P., & Duran, R. B. 2009, MNRAS, 400, 75
Kumar, P., Hernandez, R. A., Bosnjak, Z., & Duran, R. B. 2012, MNRAS, 427, L40
Margutti, R., Alexander, K. D., Xie, X., et al. 2018, ApJL, 856, L18
Mirzoyan, R. 2019, ATel, 12390, 1
Mooley, K. P., Deller, A. T., Gottlieb, O., et al. 2018, Natur, 561, 355
Mooley, K. P., Frail, D. A., Dobie, D., et al. 2018, ApJL, 868, L11
Nynka, M., Ruan, J. J., Haggard, D., & Evans, P. A. 2018, ApJL, 862, L19
Parsons, R. D., & Hinton, J. A. 2014, APh, 56, 26
Piro, A. L., & Kollmeier, J. A. 2018, ApJ, 855, 103
Rees, M. J., & Meszaros, P. 1992, MNRAS, 258, 41
Rodrigues, X., Biehl, D., Boncioli, D., & Taylor, A. M. 2019, APh, 106, 10
Rolke, W. A., López, A. M., & Conrad, J. 2005, NIMPA, 551, 493
Savchenko, V., Ferrigno, C., Kuulkers, E., et al. 2017, ApJL, 848, L15
Takami, H., Kyutoku, K., & Ioka, K. 2014, PhRvD, 89, 063006
Troja, E., Piro, L., van Eerten, H., et al. 2017, Nature, 551, 71
Troja, E., Ryan, G., Piro, L., et al. 2018, NatCo, 9, 4089
Villar, V. A., et al. 2017, ApJL, 851, L21